Deciphering the quantitative relationship between NRF2 and SRXN1 through semi-mechanistic computational modeling

Sharma, R.P.; Loonstra-Wolters, L.; Braak, S.J. ter; Niemeijer, M.C.; White, A.; Water, B. van de; ... ; Beltman, J.B.

Toxicology 519 (2026) 154284

Contents lists available at ScienceDirect

Toxicology

journal homepage: www.elsevier.com/locate/toxicol

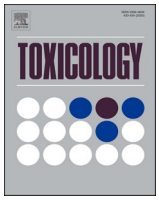

Deciphering the quantitative relationship between NRF2 and SRXN1 through semi-mechanistic computational modeling

Raju Prasad Sharma [a], Liesanne Loonstra-Wolters [a], Bas ter Braak [a], Marije Niemeijer [a], Andrew White [b], Bob van de Water [a], Alistair M. Middleton [b], Joost B. Beltman [a,*]

[a] Division of Cell Systems and Drug Safety, Leiden Academic Centre for Drug Research, Leiden University, Einsteinweg 55, Leiden 2333 CC, the Netherlands
[b] Safety, Environmental and Regulatory Science, Unilever, Colworth Science Park, Sharnbrook, Bedford MK44 1LQ, UK

ARTICLE INFO

Handling Editor: Dr. Mathieu Vinken

Keywords:
NRF2
SRXN1
Chemical exposure
Repeated exposure
Hepatotoxicity
Nonlinear mixed effect modeling

ABSTRACT

Nuclear factor erythroid 2-related factor 2 (NRF2) plays a vital role in the regulation of various antioxidant response element (ARE) genes, which control physiological processes such as oxidative stress, autophagy, proliferation and apoptosis to maintain cellular homeostasis. It is not understood in detail how the NRF2 program acquires its flexibility with respect to regulation of its downstream targets. Various NRF2 binding partners and cofactors specific to ARE genes are involved in this regulation, and are potentially condition-specific (e.g., type of stressor) and dependent on non-canonical signaling pathways (i.e., crosstalk). Here, we explored the quantitative relationship between NRF2 and sulfiredoxin 1 (SRXN1), a bona fide key NRF2 target gene. We developed a semi-mechanistic mathematical model based on time course experimental data of NRF2 and SRXN1 protein expression in HepG2 cells following single or repeated exposure to NRF2 activating soft electrophiles (sulforaphane, andrographolide, ethacrynic acid or CDDO-me) at a wide concentration range. We showed that a nonlinear mixed effect modeling approach with partially hierarchical parameters accurately captures the observed experimental dynamics. Our analysis highlights that NRF2 requires a cofactor or post-translational modification to regulate its activity as a transcription factor. Moreover, this modulation of the transcription factor activity of NRF2 is time-, compound- and exposure scenario specific. We conclude that a complete understanding of NRF2-mediated ARE genes activation requires detailed dynamic information on NRF2 binding partners and cofactors.

1. Introduction

Hepatotoxicity is a leading cause of adversity, frequently resulting in failure of preclinical and clinical trials due to drug-induced liver injury (DILI) (Centers et al., 2002; Kaplowitz, 2001). Various cellular stress signaling pathways, such as the oxidative stress response (OSR), the inflammatory stress response (ISR), the unfolded protein response (UPR), and the DNA damage response (DDR) have been implicated in DILI, and the mechanism through which these pathways are activated by exposure to a chemical or drug determines whether the liver injury is acute or chronic (Pickering et al., 2013). Among the mentioned pathways, the OSR plays a particularly prominent role in DILI (Ghanim et al., 2021), as it swiftly responds to chemical stress and tightly regulates several key physiological processes, i.e., autophagy, proliferation, and apoptosis.

The main transcription factor within the OSR is Nuclear factor erythroid 2-related factor 2 (NRF2; gene name *NFE2L2*). Under homeostatic conditions, most of the synthesized NRF2 protein is sequestered in the cytosol by actin-associated Kelch-like ECH associated protein 1 (KEAP1), and subsequent ubiquitination of NRF2 leads to its degradation by the proteasome (Suzuki and Yamamoto, 2015; Yamamoto et al., 2018). Upon exposure to chemicals such as electrophilic agents, cysteine residues on KEAP1 become modified, which prevents NRF2 ubiquitination and subsequent degradation (Eggler et al., 2005). As a result, the NRF2 concentration within cells increases and NRF2 translocates to the nucleus where it binds to antioxidant response elements (AREs). This induces transcription of ARE genes such as glutamate-cysteine ligase modifier (*GCLM*), heme oxygenase 1 (*HMOX1*), NAD(P)H quinone oxidoreductase 1 (*NQO1*), thioredoxin reductase 1 (*TXNRD1*), peroxiredoxins (*PRDXs*) and sulfiredoxin1 (*SRXN1*), which play an important role in the maintenance of cellular homeostasis (Ma, 2013). SRXN1 is a key enzyme that repairs hyperoxidized peroxiredoxins, thus maintaining the antioxidant capacity of the cell (Jose et al., 2024).Finally, homeostasis is restored through the

* Corresponding author.
E-mail address: j.b.beltman@lacdr.leidenuniv.nl (J.B. Beltman).

https://doi.org/10.1016/j.tox.2025.154284
Received 31 March 2025; Received in revised form 28 August 2025; Accepted 16 September 2025
Available online 17 September 2025

effect of ARE gene regulation, and NRF2 becomes sequestered in the cytosol again. NRF2 is well recognized as a master regulator not only of the oxidative stress response (OSR), but also of the cellular response to electrophilic stress (Yamamoto et al., 2018).

Our current understanding of NRF2 as a transcriptional regulator of ARE genes remains incomplete. Specifically, it is unclear which downstream targets are preferentially activated, what their relative contributions are to the resolution of oxidative or electrophilic stress (Yamamoto et al., 2018), and to what extent these effects are chemical-specific and exposure scenario dependent. NRF2 knockout experiments have demonstrated that NRF2 is the sole transcription factor regulating ARE genes (Wijaya et al., 2022), yet regulation of such genes is complicated due to the nonlinear dynamics involved and the modifying impact of various cofactors (Reichard et al., 2007; Qian et al., 2015). Small MAF proteins (sMAFs) represent one class of cofactors that can modify transcriptional regulation mediated by NRF2 (Katsuoka et al., 2005). In homeostatic conditions, sMAFs form homodimers (Kataoka et al., 1995) but under oxidative stress conditions, sMAFs heterodimerize with NRF2, thereby enhancing its transcription factor activity (Itoh et al., 1997). The production of sMAFs, and their competition with other cofactors that heterodimerize with NRF2 (Kataoka et al., 1995) could be influenced by various biological pathways (Katsuoka and Yamamoto, 2016), possibly indicating crosstalk. Indeed, several studies reported that kinases such as ERK, PI3K, PKC and p38 MAPK modify and influence NRF2 mediated activation of downstream genes (Yu et al., 1999; Huang et al., 2000, 2002; Bloom and Jaiswal, 2003). For example, Zipper et al. reported that both ERK and the p38 pathway contribute to the transcriptional upregulation of gamma glutamylcysteine synthetase (GCS) by enhancing binding of NRF2 to ARE (Zipper and Mulcahy, 2000). Other proteins with a modifying impact are the histone acetyltransferases p300/CBP, which have been shown to directly acetylate NRF2, thereby increasing its transcription factor activity with respect to various ARE genes, such as NQO1, TXNRD1 and GCLM (Sun et al., 2009). In contrast, Reichard et al. observed that BACH1 acts as a repressor of the NRF2 target gene *HMOX1*, and inactivation of BACH1 is crucial for substantial *HMOX1* transcription (Reichard et al., 2007).

For a number of electrophilic compounds (e.g. diethyl maleate (DEM), CDDO-me, sulforaphane), we and others have demonstrated that NRF2 and its downstream molecules exhibit a concentration and compound specificity in their activation dynamics (Ke et al., 2021; Bischoff et al., 2019; ter Braak et al., 2022). The height of the perceived stress by cells may play an important role in determining these dynamics. For example, for low stress levels, peroxiredoxins (PRDXs) that scavenge ROS are preferentially activated, while for high stress levels, the detoxification capacity of PRDXs may become exhausted, resulting in hyperoxidation; under these conditions, the NRF2 target gene SRXN1 plays a crucial role in repairing over-oxidized PRDXs and restoring their antioxidant function (Jeong et al., 2012; Abbas et al., 2013). Exposure scenario and type of compound can also result in differential activation of downstream molecules. For instance, during repeated exposure scenarios we previously showed that the level of NRF2 activation was slightly lower for a second exposure than for a first exposure, yet that this resulted in a three-fold higher SRXN1 response compared to the first treatment (Bloom and Jaiswal, 2003). Moreover, this differential activation dynamics of SRXN1 upon a repeated exposure was compound specific.

Taken together, these prior findings indicate that transcription factor activity of NRF2 is influenced by various biological pathways and, considering that chemicals may perturb multiple pathways, this likely complicates NRF2-mediated regulation of various ARE genes. In order to explore the relation between NRF2 activity and ARE gene expression in a quantitative manner, we investigated the dependence of SRXN1, selected as an important NRF2 target gene, on NRF2 abundance over time following compound exposure, and studied the compound and exposure scenario dependency of this relation. We specifically asked whether the NRF2 abundance can by itself explain SRXN1 dynamics irrespective of compound type and exposure scenario, or whether there is a chemical and exposure scenario specific effect that modulates NRF2 activity.

Detailed measurements of the time-dependent induction of NRF2 under various stress conditions together with ARE gene (in this case *SRXN1*) induction along with *in silico* mechanistic modeling may provide insights into these questions. The development of quantitative high throughput imaging assays based on bacterial artificial chromosome (BAC)-transgenomics green fluorescent protein (GFP) tagging in HepG2 cells has enabled such detailed time-course dynamics of both NRF2 and SRXN1 (Bischoff et al., 2019; ter Braak et al., 2022; Wink et al., 2018, 2017). Only a limited number of *in silico* models of the NRF2 pathway response to stress have been developed (Kolodkin et al., 2020; Zhang and Andersen, 2007; Khalil et al., 2015; Leclerc et al., 2015; Hiemstra et al., 2022), and these models have not been applied to study compound and exposure scenario dependence of the relation between NRF2 and SRXN1. Therefore, we set out to develop a semi-mechanistic model that could be applied to high throughput imaging data based on multiple compounds and repeated exposure data of NRF2 and SRXN1 using HepG2 BAC GFP reporter cells. Our approach utilizes nonlinear mixed-effect models aiming to predict SRXN1 dynamics based on a known input of NRF2 dynamics. We considered four electrophilic compounds, i.e. sulforaphane (Sul), andrographolide (Andr), ethacrynic acid (ETA) and CDDO-me (CDDO), which were already known to activate the NRF2 pathway (ter Braak et al., 2022). We fitted our models to data of HepG2 cells that were exposed to these chemicals in an *in vitro* setting. We showed that modulators are required which modify the transcription factor activity of NRF2, and that the activity of these modulators should vary both over time and with compound and exposure scenario.

2. Methods

2.1. Experimental data and analysis

The data for our study was obtained from assays performed with HepG2 NRF2 and SRXN1 BAC-GFP reporter cell lines (Ke et al., 2021; Bischoff et al., 2019; Hiemstra et al., 2022). Live cell imaging using confocal microscopy was used to determine the NRF2 and SRXN1-GFP responses over time upon exposure to various chemicals, considering multiple stress conditions (i.e., single or repeated exposure). For further experimental details, see (ter Braak et al., 2022; Niemeijer et al., 2025). In brief, for every HepG2 BAC-GFP reporter, we generated three biological replicates each consisting of two technical replicates for which we took two images from different positions of the same well upon compound exposure. Subsequently, the GFP intensities in generated images were quantified in a specific subcellular location using an automated pipeline consisting of ImageJ plugins and CellProfiler 2.2.0 modules as reported previously (Sun et al., 2009; Bischoff et al., 2019). Individual nuclei were segmented based on the Hoechst signal as reported previously (Bois and Maszle, 1997). This allowed the quantification of nuclear NRF2 intensity by the calculation of the integrated NRF2-GFP intensity of all pixels belonging to a detected nucleus, and subsequently taking the arithmetic mean of all nuclei in an image. Similarly, integrated cytoplasmic SRXN1-GFP intensities of individual cells were determined by utilizing the Identify-secondary-objects module set to the ‘propagation’ distance-N method (using 20 pixels) in CellProfiler.

Four different compounds were studied: Sul, Andr, ETA and CDDO, along with DMSO as a control. For Sul and CDDO, we re-used our published experimental data (Niemeijer et al., 2025), while the data for Andr and ETA were generated as part of the current work. We exposed HepG2 NRF2 or SRXN1 BAC-GFP reporter cell lines to these compounds at different concentrations ranging from subthreshold to maximally effective concentrations as known from prior studies (Bischoff et al.,

2019; ter Braak et al., 2022) (Table 1). All compounds were freshly prepared in DMSO and added to the culture medium immediately prior to exposure (Bischoff et al., 2019). These compounds are expected to remain sufficiently stable and bioactive under cell culture conditions for the duration of the experiments. However, measurements of compound concentrations in the medium have shown that there are clear differences in compound stability, with CDDO concentrations being the most stable (Niemeijer et al., 2025). We applied two continuous exposure scenarios (32 h and 48 h single exposure), and two repeated exposure scenarios (8 h first exposure followed by medium change and 24 h second exposure, referred to as 8 h + 24 h; and 24 h first exposure followed by medium change and then 24 h exposure, referred to as 24 h + 24 h). For the repeated exposure scenarios, we applied all possible combinations of concentrations in the first and second exposure. During the imaging, the plates were taken out of the microscope for the second exposure. Note that this resulted in some additional NRF2 activation also for the wells with continuous single exposure, possibly due to minor handling-related stress.

After quantification of GFP intensities through our image analysis pipeline, we averaged the two technical replicates, forming one biological replicate for every time point. Then we normalized the data for each biological replicate based on the DMSO control, which was done by subtracting the GFP intensity of chemical-treated cells with DMSO-treated cells for every time point. First this was done separately for each concentration and each biological replicate. Subsequently the mean intensity per time point was calculated across all biological replicates. The time course of this mean at concentration 6 (see Table 1) for each chemical was utilized to generate a hysteresis plot (i.e., plotting the SRXN1-GFP intensity against NRF2-GFP), thereby providing insight into the NRF2-SRXN1 relationship, such as the occurrence of delays. Note that at the studied concentrations (Table 1), there was a similar increase in cell counts over time for all our chemicals, with only a slightly slower increase rate at the highest utilized concentrations (Andr and ETA, see Fig. S1; Sul and CDDO, see (Niemeijer et al., 2025).

2.2. Model design

We created three different model versions in order to establish the mechanistic relationship between NRF2 and SRXN1, i.e., (1) a model with constant NRF2 transcription factor activity, (2) a model with constant cofactors (not described explicitly) modifying NRF2 transcription factor activity, hereafter referred to as 'cofactor X' (where X represents a hypothetical set of cofactors or NRF2 modifiers), and (3) a model with a dynamic cofactor X (i.e., whose activity or expression varies over time) modifying NRF2 transcription in a time-dependent manner. All model versions use NRF2 time course experimental data as inputs. To this purpose, we transformed the NRF2 time course data into a smooth time-dependent input $N(t)$ using the R spline function, because a smooth function is required by the internal steps taken by ODE integration algorithms.

The Ordinary differential equation (ODE) for SRXN1 (S) in the 3 considered models includes basal production and degradation of SRXN1, and NRF2-induced SRXN1 production (Eq. I).

$$\frac{dS}{dt} = k_p - k_d * S + p_s \quad \text{(I)}$$

Here, k_p is the basal SRXN1 production rate, k_d is the basal SRXN1 degradation rate, and p_S is the NRF2-induced SRXN1 production rate.

2.2.1. Model with constant NRF2 transcription factor activity

In the simplest model version (Fig. 1A), we considered NRF2-mediated SRXN1 transcription to be independent of activity of cofactor X. Specifically, the NRF2-induced SRXN1 production rate (p_S) depends on NRF2 ($N(t)$) following a nonlinear Hill process:

$$p_S = \frac{(V_{max} * N(t)^n)}{(K_m{}^n + N(t)^n)} \quad \text{(II)}$$

Here, V_{max} is the maximal SRXN1 production rate, K_m is the NRF2 level for which the SRXN1 production rate is half-maximal, and n is the Hill coefficient.

2.2.2. Model with a constant cofactor X modifying NRF2 transcription factor activity

Next, we considered that cofactor X (representing a set of cofactors or NRF2 modifiers, for example CREB-binding protein (CBP), p300, p160, and receptor-associated co-activator 3 (RAC3)) modifies the transcription factor activity of NRF2, which would affect a subset of the present NRF2. Thus, at each time point the total NRF2 is split in an amount of modified NRF2 (N_m) and of unmodified NRF2 (N_u) due to the presence of cofactor X (Fig. 1B). These amounts are determined by parameter f, which represents the fraction of NRF2 whose transcription is affected by cofactor X ($0 \leq f \leq 1$):

$$N_m(t) = N(t) * f;\ N_u(t) = N(t) * (1 - f). \quad \text{(III)}$$

We described the NRF2-induced SRXN1 expression by a multiplicative mechanism, i.e. the presence of both unmodified and modified NRF2 provides increased stimulation of SRXN1 production in a nonlinear manner:

$$p_s = \frac{(V_{max1} * N_m{}^{n_m} * N_u{}^{n_u})}{(K_{m_m}{}^{n_m} + N_m{}^{n_m}) * (K_{m_u}{}^{*n_u} + N_u{}^{n_u})}. \quad \text{(IV)}$$

Here, V_{max1} is the maximum induction rate of SRXN1 by NRF2, K_{m_m} and K_{m_u} are the Michaelis-Menten constants for the modified and unmodified NRF2, respectively, and n_m and n_u for the Hill coefficients of modified and unmodified NRF2, respectively.

2.2.3. Model with a dynamic cofactor X modifying NRF2 transcription factor activity

Finally, we considered that cofactor X might have its own dynamic response to the applied chemicals, which would also make the fraction of modified NRF2 vary with time. Modeling the dynamics of cofactor X with a separate ODE would require assumptions on both its production and degradation processes, as well as on its modification of NRF2, which would be problematic for parameter calibration in the absence of data on either of these aspects. Therefore, we focused on directly describing the dynamics of the fraction of modified NRF2 in a semi-mechanistic manner, anticipating that this fraction would initially increase due to compound exposure, and after reaching a maximum would decrease again. Moreover, second dosing would lead to another increase and subsequent decrease, albeit with a different initial fraction and potentially different increase and decrease parameters. To model this semi-mechanistically, we extended the prior model version by making the fraction of modified NRF2 dynamic instead of constant (as in Eq. IV) with only a limited number of additional parameters:

Table 1
The different exposure scenarios per compound to which HepG2 cell lines were exposed.

Compound	Concentration(μM)	1	2	3	4	5	6
Sulphoraphane (Sul)		0.35	0.75	1.62	3.5	7.54	16.25
Andrographolide (Andr)		0.1	0.32	1	3.16	10	31.62
Ethacrynic Acid (ETA)		1	2.14	4.64	10	21.54	46.4
CDDO-me (CDDO)		0.01	0.02	0.05	0.1	0.22	0.46

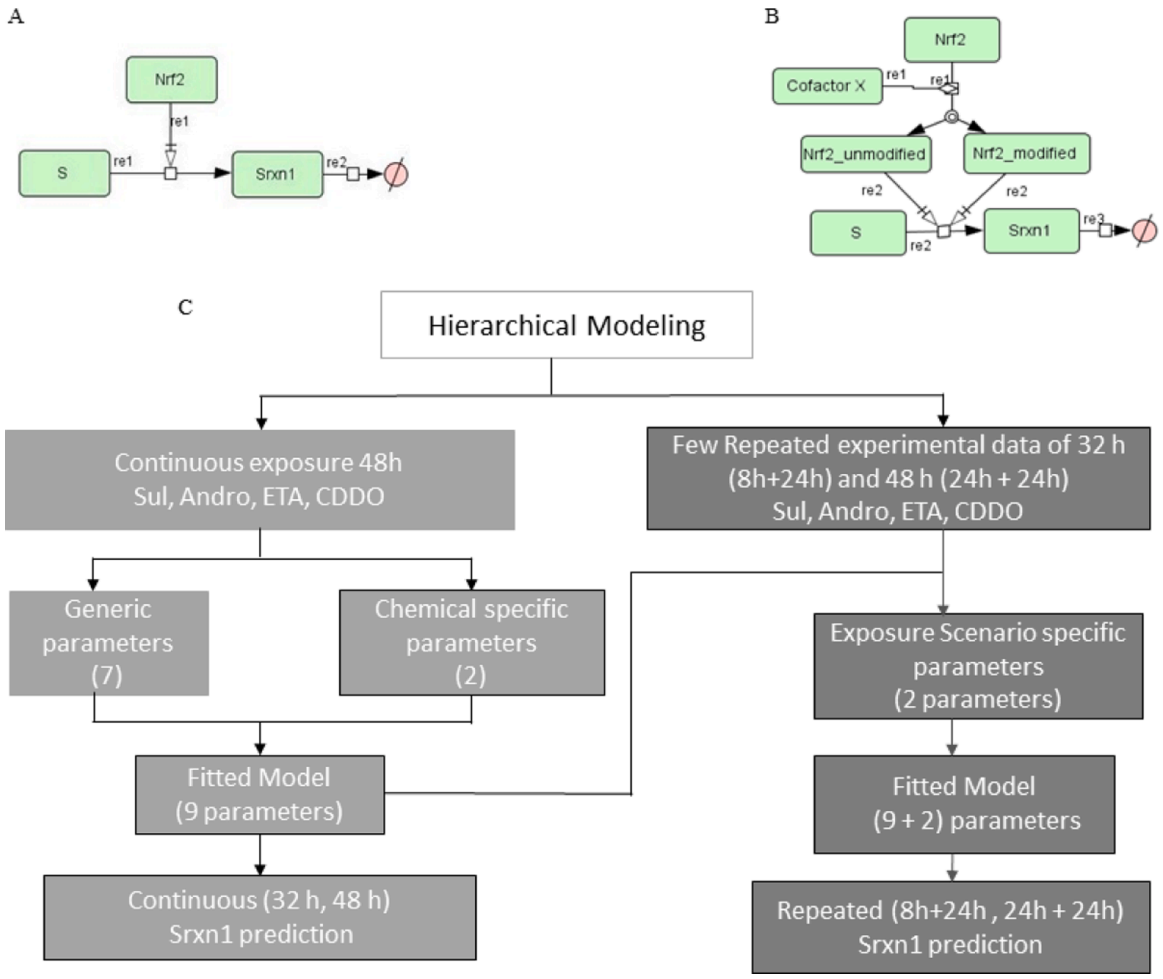

Fig. 1. *Modeling strategy to describe SRXN1 dynamics induced by NRF2.* A-B) Schematics of model with constant NRF2-mediated induction of SRXN1 transcription (A) and of two models with modified NRF2 having distinct effects on SRXN1 transcription compared to unmodified NRF2 (B). In (B), implicitly described NRF2 modifiers are considered to affect the fraction of modified NRF2 (potentially in a dynamic manner), which in turn influences SRXN1 transcription. In all model versions, SRXN1 undergoes basal degradation. C) Nonlinear mixed modelling framework: Panel summarizes which data are utilized for which generic and chemical- or exposure-scenario-specific parameters within our Bayesian framework.

$$f = \frac{1}{\left(\frac{1}{f_i} - 1\right) * \exp(-t * r_1) + \exp(t * d_1)} \{t \geq t_{dosing1}, t < t_{dosing2}\}$$

$$f = \frac{1}{\left(\frac{1}{f_i} - 1\right) * \exp(-t * r_2) + \exp(t * d_2)} \{t \geq t_{dosing2}\}, \text{ with}$$

$$f_1 = \frac{1}{\left(\frac{1}{f_i} - 1\right) * \exp\left(-t_{dosing2} * r_1\right) + \exp\left(t_{dosing2} * d_1\right)}. \quad \text{(V)}$$

Here, t represents time since first dosing at $t_{dosing1} = 0$, and the second dosing (if applicable) occurs at time point $t_{dosing2}$. Further, r_1 and r_2 determine the rates at which cofactor X increases after a first and a second dosing, respectively, d_1 and d_2 determine the rates at which cofactor X decreases after a first and a second dosing, respectively. Finally, f_i and f_1 represent the initial fraction and fraction prior to second dosing of modified NRF2 due to cofactor X respectively.

2.3. Parameter calibration

The model parameters were calibrated to our experimental data with a Bayesian approach, implemented in MCSim (ver. 6.1) (Vehtarh et al., 2021). In this approach, parameter values are considered random variables distributed either according to a normal distribution or a truncated normal distribution. In conjunction with a likelihood function, we determined posterior distributions by Markov Chain Monte Carlo (MCMC) simulations. The likelihood of the data was considered to follow a normal distribution with a coefficient of variation of 10 %. We initialized the variable S (SRXN1) at a value determined by the ratio between its basal synthesis rate (k_p) and degradation rate (k_d) to ensure that the model starts at steady state. Further, we constrained these two parameters by using a truncated normal prior distribution within the range 1e-4 to 1 for k_p, and 1e-4 to 1 for k_d. We have also constrained the Hill coefficients (n_m and n_u) within the range 1 to 10 using the same approach. We did this to avoid the possibility of very large Hill coefficients that would approximate a step function on the one hand, and to remain in a regime of biologically interpretable Hill coefficients (i.e., at least 1) on the other hand. We ran four independent Markov chains of 100,000 to 1,000,000, and used the last 10,000 iterations to check convergence with the potential scale reduction factor $\hat{R}$. This includes a joint prior distribution of the parameters which is randomly sampled within the given distribution and eventually gets updated through a comparison of model predictions and the experimental data. The convergence criterion $\hat{R}$ was computed for the four different chains and all values were below 1.05 indicating model convergence (Hsieh et al., 2020). All model parameters were estimated simultaneously, and we did not observe evidence of non-identifiability or practical estimation issues

based on MCMC convergence and pairwise posterior plots (Fig. S2). It should be noted that the latter analysis did indicate some naturally expected yet moderate parameter dependencies, e.g. between the SRXN1 production rate (k_p) and degradation rate (k_d).

For the simplest model with constant NRF2 transcription factor activity (model 1), we fitted the parameters using only the 48 h continuous exposure data for Sul. Subsequently, the model with the estimated parameters, i.e., k_p, k_d, V_{max}, K_m, n was simulated for the other three compounds using their respective experimental NRF2 time course data as inputs. For the model with a constant cofactor X modifying NRF2 transcription factor activity (model 2), we kept some parameters the same for all chemicals, i.e., k_p, k_d, V_{max1}, K_{m_m}, K_{m_u}, n_m, n_u. The cofactor X that modifies NRF2 transcription factor activity was considered compound-specific, leading to a constant fraction of modified NRF2 (parameter f). We fitted the parameters using the 48 h continuous exposure data for all four compounds in a hierarchical fashion (with f a hierarchical parameter).

For the model with a dynamic cofactor X modifying NRF2 transcription factor activity (model 3), the prior model was extended by considering that the dynamic response of cofactor X leads to a fraction of modified NRF2 that varies over time. The parameters determining this response, i.e., r_1, r_2, d_1, d_2 (Eq. V) were both compound- and exposure scenario-specific. We used the following calibration strategy (Fig. 1C): First we fitted all the parameters using the 48 h continuous exposure data for all four compounds. For parameters r_1, r_2, d_1, d_2, we used a hierarchical specification. Population-level parameters (r_{1all}, r_{2all}, d_{1all}, d_{2all}) describe the overall parameter space across compounds, while compound-specific parameters (r_1, r_2, d_1, d_2) are modeled as draws from this shared space. During MCMC sampling, both levels are estimated jointly, so the inference yields posterior estimates for the population parameters as well as for each compound-specific parameter. Subsequently, both compound- and scenario-specific parameters were estimated using the experimental data from the exposure combinations where the first exposure ranges from lowest to highest and the second exposure was the highest concentration. Note that this was done separately for the 32 h (8 h+24 h) and 48 h (24 h+24 h) exposure data, while using the same model structure and keeping the other parameters to the same value. The estimated model parameters and their meaning for the different model versions are provided in Tables S1-S3.

2.4. Model diagnostics

The model with a dynamic cofactor X was used to predict various continuous and repeated exposure scenarios. For these model simulations, we used three different NRF2 inputs to predict SRXN1. Specifically, these inputs included the mean, maximum and minimum of NRF2 per time point on the basis of the three biological replicates. Finally, we visually compared the model simulations to the experimental data of various scenarios and different concentration combinations. Importantly, a large amount of these combinations were not used during parameter calibration.

Apart from visual comparison of model predictions and experimental data, we also calculated R^2 for the different model versions. To investigate the effect of parameter variation on model output, we employed a global sensitivity analysis (GSA) using the R package pksensi (Louizos et al., 2014). This package uses a variance-based GSA method that integrates random phase-shift with extended Fourier Amplitude Sensitivity Test (eFAST) to perform the sensitivity test (Hsieh et al., 2020). All parameters were varied by 1 % to compute the effect on the SRXN1 response and sensitivity coefficients over time were calculated for each parameter. Sensitivity coefficients higher than 0.1 were considered to indicate highly influential parameters, and lower than 0.05 were considered non-influential parameters.

3. Results

3.1. NRF2 regulates SRXN1 in a compound-specific manner

Plots of NRF2-GFP expression versus SRXN1-GFP expression at the same time points (Fig. 2A-B; Fig. S3A-B) as well as plots of NRF2-GFP expression and SRXN1-GFP expression over time (Fig. 2C-D; Fig. S3C-D) upon compound exposure demonstrated that SRXN1 expression increased in a delayed manner relative to the NRF2 expression increase, a phenomenon described by the term 'counter-clockwise hysteresis (Louizos et al., 2014). This implies that the relation between NRF2 and SRXN1 may not be adequately captured by a simple linear function, which motivated our use of nonlinear models in subsequent quantitative analysis. The dynamics of fast NRF2 activation followed by delayed SRXN1 activation occurred for all considered compounds. Curve shifts to the left and upwards at late time points indicated that NRF2 expression decreased at late time points yet that SRXN1 expression was still increasing upon continuous exposure of 32 h, except for exposure to Andr for which a minor SRXN1 decay occurred (Fig. 2A). During longer time periods of continuous exposure (48 h), for ETA and Sul an SRXN1 plateau was reached, yet for CDDO SRXN1 still continued to increase (Fig. 2B).

For repeated exposure scenarios of 32 h (8 h + 24 h; Fig. S3A) and of 48 h (24 h + 24 h; Fig. S3B), the overall patterns did not change compared to the continuous exposure scenarios. For exposure to CDDO, both SRXN1 and NRF2 reached similar maximal levels for repeated and single exposure (Fig. S3A-B vs Fig. 2A-B, yellow). For the other compounds, both NRF2 and SRXN1 obtained somewhat higher levels at the end of the observation period (48 h) for repeated than for single exposure. For exposure to Sul a minor SRXN1 decay occurred during the second exposure after a 24 h initial exposure (Fig. S3A, grey). Thus, at the highest administered concentration there were clear differences in the qualitative relation between NRF2 and SRXN1 across compounds, which persisted for both single and repeated exposure scenarios. This suggests that the regulatory role of NRF2 may be different depending on the compound that activates the oxidative stress pathway.

3.2. Mathematical modeling confirms chemical dependence of NRF2-mediated SRXN1 regulation

In order to investigate whether the observed difference of the temporal relation between nuclear NRF2 expression and SRXN1 expression across compounds at the highest applied concentrations hold true for other concentrations as well, we employed a semi-mechanistic mathematical modeling approach. Specifically, we utilized a simple ordinary differential equation (ODE) for NRF2-driven SRXN1 expression including nonlinear Hill kinetics (referred to as model with constant NRF2 activity), where we took the measured NRF2 expression as a concentration- and compound-dependent input function over time estimated by spline interpolation (see Methods). We started with formal estimation of the parameters related to SRXN1 formation and degradation for Sul based on 48 h continuous exposure data (Fig. S4A, S5B; see Table S1 for model parameters). Among the six applied concentrations, the model with constant NRF2 activity resulted in an acceptable match to the three highest concentrations (Fig. 3A, top panel). For the lowest three concentrations, the fit was clearly worse compared to the three highest concentrations, and the long-term SRXN1 dynamics were overestimated (Fig. 3A, bottom panel). Notably, the initial Hill model estimated a Hill coefficient close to 1 and a very large K_m value, corresponding to a nearly linear response. This suggests that even for application of a single compound, the effect of NRF2 as a transcription factor differs for high and low concentrations at which the compound is applied.

Subsequently, we simulated the same model for the other compounds using the fitted parameters for Sul yet the NRF2 input for the individual compounds. For all compounds, the model simulations

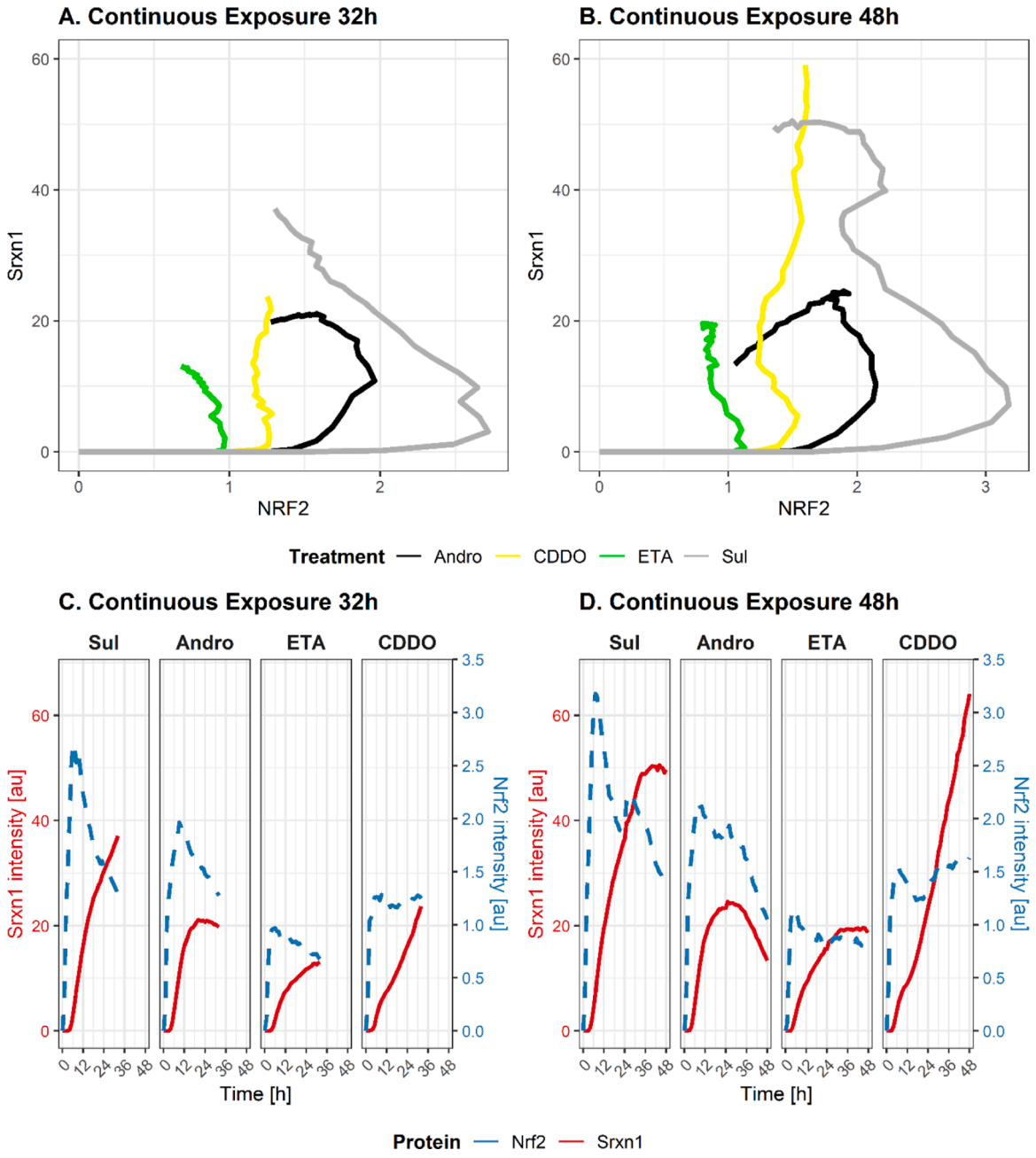

Fig. 2. *Quantitative relation between NRF2 and SRXN1 is compound dependent.* (A-B) Plots show SRXN1-GFP expression vs NRF2-GFP expression in HepG2 BAC reporter cells upon continuous exposure for 32 h (A) and 48 h (B) to the compounds Andr, CDDO, ETA or Sul (colors) at a concentration of 31.62, 0.46, 46.4 or 16.25 μM, respectively. (C–D) Time courses of SRXN1-GFP (solid red, left y-axis) and NRF2-GFP (dashed blue, right y-axis) for the same exposures over 32 h (C) and 48 h (D). Intensities are in arbitrary units (au).

exhibited either over- or underestimation of the experimental data (Fig. 3B-D). In particular, the model was not able to predict the SRXN1 decay observed at late time points for Andr and ETA, leading to an overestimation of SRXN1 dynamics (Fig. 3B-C). To the contrary, for CDDO-me the model underestimated the SRXN1 response at the highest concentrations (Fig. 3D). This is consistent with the observation that the maximum expression of NRF2 was approximately 2-fold less for CDDO compared to Sul at the highest concentration, whereas the SRXN1 expression was similar (Fig. 3A-B). Together, these findings indicate that the transcription factor activity of nuclear NRF2 is both concentration- and compound-dependent. As a result, straightforward Hill kinetics is not sufficient to capture this differential regulatory effect of NRF2 on SRXN1.

3.3. A fixed fraction of modified NRF2 improves fit of concentration-dependent SRXN1 expression

Because several cofactors/regulators (jointly referred to as cofactor X) can play a role in promoting or inhibiting NRF2 transcriptional activity, e.g., through acetylation of NRF2 by p300/CBP, we considered the possibility that a fixed fraction of the present NRF2 is in modified form due to presence of cofactor X, and therefore has altered transcription factor activity. Thus, in a subsequent model version, referred to as the model with fixed cofactor X, we split the present NRF2 in two fractions which together determine SRXN1 transcription (see Eqs. III & IV in Methods). In addition, we considered the possibility that the fraction of modified NRF2 due to cofactor X could depend on the type of compound, because they may have multiple modes-of-action. Thus, the

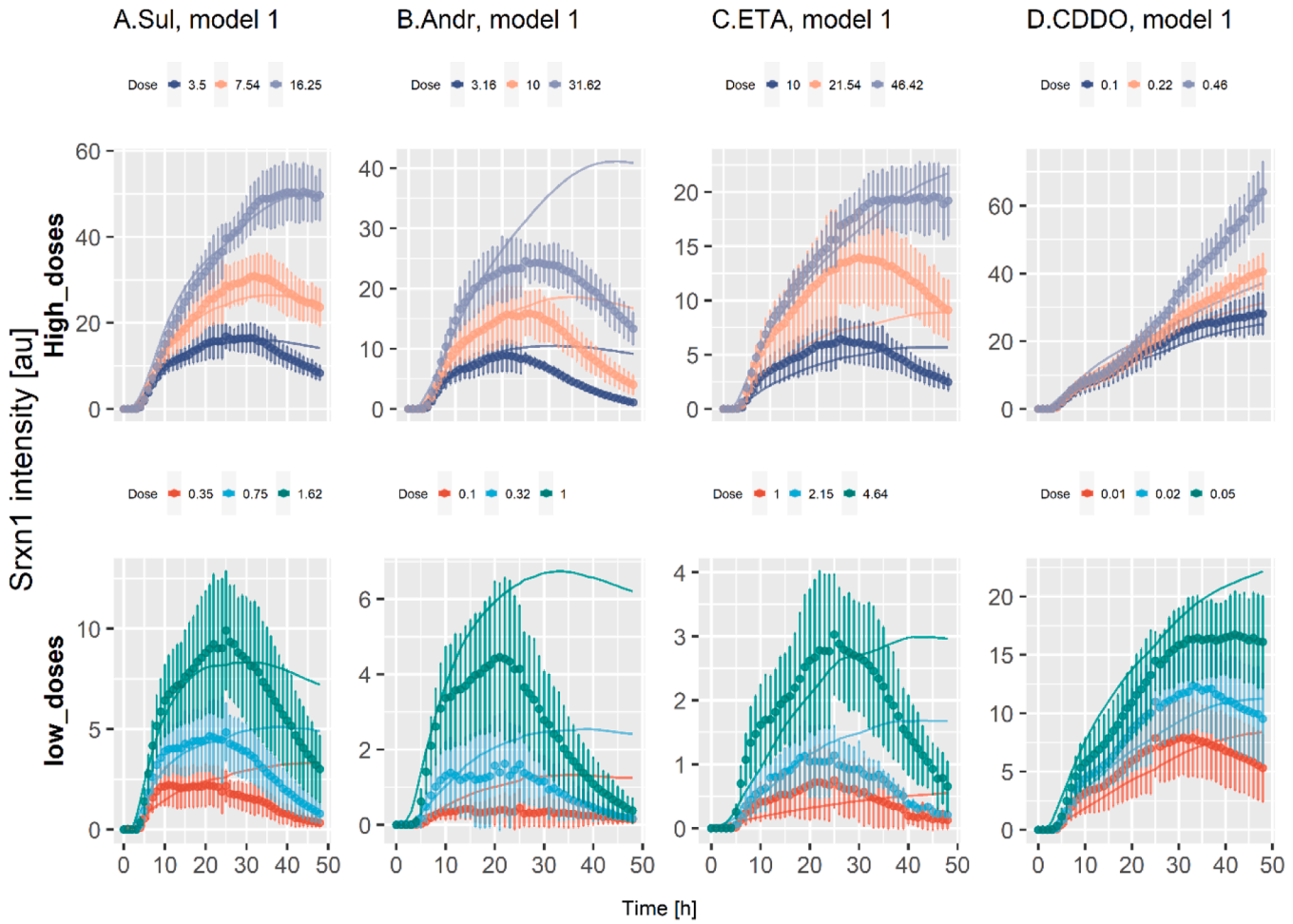

Fig. 3. *Nonlinear Hill kinetics do not capture NRF2-mediated SRXN1 regulation across concentrations and compounds.* A-D) Panels show experimental measurements (mean ± sd (from three biological replicates)) and model fit (solid lines) of SRXN1 expression in HepG2 BAC-GFP reporter cells for Sul (A), Andr (B), ETA (C) and CDDO (D) at either high concentrations (top panels) or low concentrations (bottom panels) for up to 48 h continuous exposure. Colors denoting the administered concentration are shown at the top of the plots. Model simulations are based on the model considering a constant activity of the nuclear NRF2.

influence of cofactor X on the modified NRF2 fraction could be different for every considered compound, while the other parameters influencing SRXN1 dynamics were shared for all chemicals.

Calibration of the model with fixed cofactor X (Fig. S4B; see Table S2 for model parameters) slightly improved the fit (Fig. 4) compared to the earlier model with constant NRF2 activity (Fig. 3). Specifically, for Sul the R^2 value was larger than 0.8 at both high and low concentrations (Fig. 4A), and for the other compounds R^2 was larger than 0.6 except for Andr which had $R^2 < 0.6$ at low concentrations (Fig. S5). Clearly, despite the improved fit this model still had difficulties with capturing the decreasing SRXN1 dynamics at late time points, suggesting that the remaining nuclear NRF2 at those points might exhibit less transcription factor activity than in the early response.

3.4. A dynamic fraction of modified NRF2 explains compound-specific and exposure scenario-specific SRXN1 response

Modifiers and cofactors of NRF2 that influence its activity as a transcription factor might themselves exhibit a dynamic response pattern when exposed to specific compounds. Therefore, we considered the possibility that the fraction of modified NRF2 initially increased and subsequently decreased during the waning of the response, and that this dynamic pattern was compound dependent. Thus, we constructed a third model version, referred to as the model with dynamic cofactor X (see Eq. V in Methods), in which the initial fraction of cofactor X was set to a very low level (1e-3) that initially increased (described with parameter r_1) and later on decreased (described with parameter d_1). In this model, r_1 and d_1 were considered to be compound-specific, whereas the other parameters for SRXN1 production and decay were shared across compounds.

Calibration of this model with dynamic cofactor X to the 48 h continuous exposure SRXN1 data (Fig. S6; see Table S3 for model parameters) led to a much better fit (Fig. 5) than the simpler models (Figs. 3–4). To take into account the biological variability among replicates, we simulated the calibrated model using minimal, mean, and maximal inputs for NRF2 (Fig. S7). To check for consistency across data sets, we also simulated the model for the shorter-lasting 32 h continuous exposure scenario while keeping all parameters at the same value. This showed that the model also properly predicted the 32 h continuous exposure scenario data (Fig. S8), providing further confidence in the model. Importantly, the model simulations now captured the SRXN1 decay also at late time points. Although for some concentrations the model slightly over- or underestimated the experimental data, for each compound the R^2 value exceeded a value of 0.9, demonstrating the goodness-of-fit of this model quantitatively (Fig. S9).

Having a model that properly describes the relation between NRF2 and SRXN1 based on a dynamic fraction of modified NRF2, we next considered whether the model could also describe various repeated exposure scenarios for the same compounds. We reasoned that upon a second exposure the fraction of modified NRF2 should again change

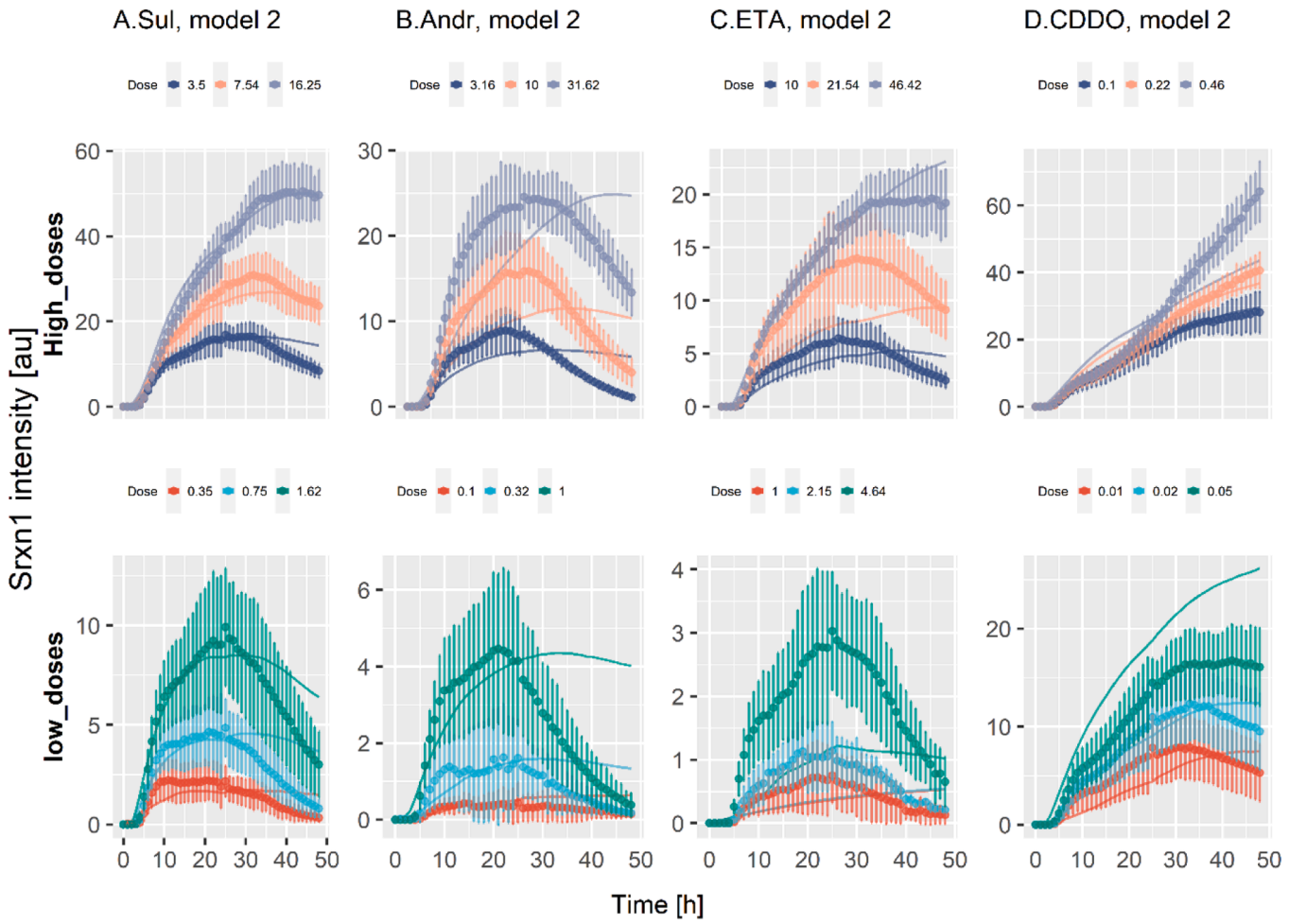

Fig. 4. Fit of model with fixed fraction of modified NRF2 due to cofactor X to observed SRXN1 intensities. A-D) Panels show experimental measurements (mean ± sd of three biological replicates) and model fit (solid lines) for Sul (A), Andr (B), ETA (C) and CDDO (D) at either high concentrations (top panels) or low concentrations (bottom panels). Colors denote the administered concentration (μM) and their values are shown at the top of the plots.

with time. However, the starting point of the fraction of modified NRF2 should be different at the time of second exposure given its dynamic change throughout the primary exposure. Therefore, it was likely that the increase and decay dynamics of the fraction of modified NRF2 would also deviate from the first exposure. Therefore, to describe repeated exposure data we included two additional parameters in the model describing the increase (r_2) and decrease (d_2). We calibrated the additional parameters on the basis of a selected set of concentration combinations (see Methods), while keeping the other parameters to the values resulting from the fit of the first exposure. We simulated the model with newly calibrated r_2 and d_2 parameters for all four compounds and all repeated exposure scenarios (Fig. S10-S17). A subset of the repeated exposure scenarios, i.e., with repeated 48 h (24 h+24 h) and 32 h (8 h+24 h) scenario with equal concentrations during first and second exposure, and with large differences between the concentrations of first and second exposure demonstrated that the model fit was generally good (Fig. 6). This evaluation by visual inspection was confirmed by R^2 values that typically exceeded 0.9 for 32 h repeated exposure data and 0.8 for 48 h repeated exposure data (Fig. S18). Only for a limited number of concentration combinations clear over- and under-predictions occurred. In conclusion, on top of the proper description for single exposure scenarios, the model with dynamic cofactor X could explain a large number of repeated exposure dosing schemes (384 combinations in total). Importantly, to achieve this per compound, only one additional process was required, involving 2 parameters for continuous exposure scenarios and 2 additional parameters for repeated exposure scenarios.

3.5. *Mechanistic insight based on model with dynamic fraction of modified NRF2*

In the model with a dynamic fraction of modified NRF2, we considered that a fraction of the present NRF2 becomes modified. The modified NRF2 is assumed to have greater transcriptional activity when compared to unmodified NRF2. A fast modification process would imply that the molecules (cofactors) playing a role in the modification follow a similar time course as that of modified NRF2. Thus, studying how the time course of modified NRF2 depends on the chemical and on the exposure scenario provides mechanistic insight. The shape of the curve, i.e., the extent of activation and decay, and the different dynamics for first and second exposures represent the characteristic features of the response (Fig. 7A). A large fold increase in modified NRF2 and a large area under the curve suggests a strong involvement of modification enzymes or cofactors in the transcription factor activity of NRF2 with respect to SRXN1.

Treatment with Sul caused most NRF2 modification compared to the other compounds, whereas Andr treatment led to the lowest amount of NRF2 modification. For CDDO, the decay rate of modified NRF2 was lower than for other compounds, which is consistent with the high stability of CDDO (Niemeijer et al., 2025). For all compounds, second exposures led to an increased fraction of modified NRF2 compared to continuous exposure, yet the extent of the increase depended on the

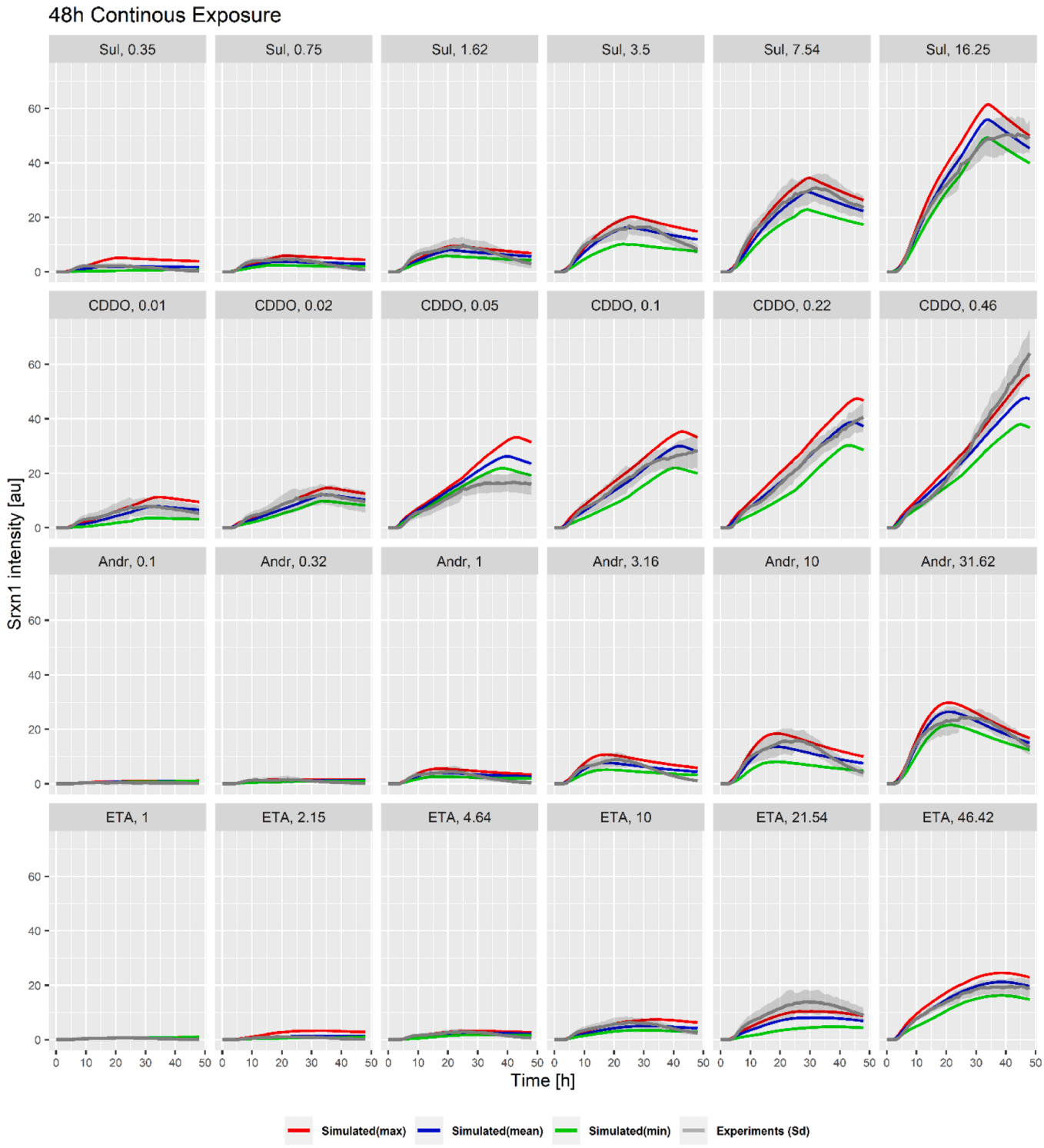

Fig. 5. Model with dynamic cofactor X describes SRXN1 dynamics following continuous exposure. Plots show simulated SRXN1 expression upon compound exposure based on minimal (green), maximal (red) and mean (blue) NRF2 input per time point, and experimentally determined SRXN1 expression using HepG2 BAC-GFP reporter cells (shaded gray area: mean ± sd across three biological replicates) for 48 h. Each row corresponds to one compound (Sul, CDDO, Andr, and ETA), with exposure levels indicated above the panels (in μM).

compound and time point of second exposure. An early second exposure at the 8 h time point (Fig. 7A, red lines) typically led to modified NRF2 levels beyond the maximum observed for continuous exposure (Fig. 7A, blue lines), likely because the second exposure typically occurred at a similar time point as where this maximum occurred. However, for Sul this was not the case. Here, the amount of modified NRF2 was predicted to both increase and decrease extremely steeply, such that the moment of re-exposure at 8 h was already several hours beyond the peak. This suggests that the response of modified NRF2 during the second exposure merely caused a delay of the decrease, rather than a new peak. Interestingly, the second exposure at 24 h had only a slight effect on modified NRF2 (Fig. 7A, red lines). This suggests that NRF2-mediated transcription of SRXN1 is less strongly influenced by NRF2 modifiers for late second exposures than for primary exposures.

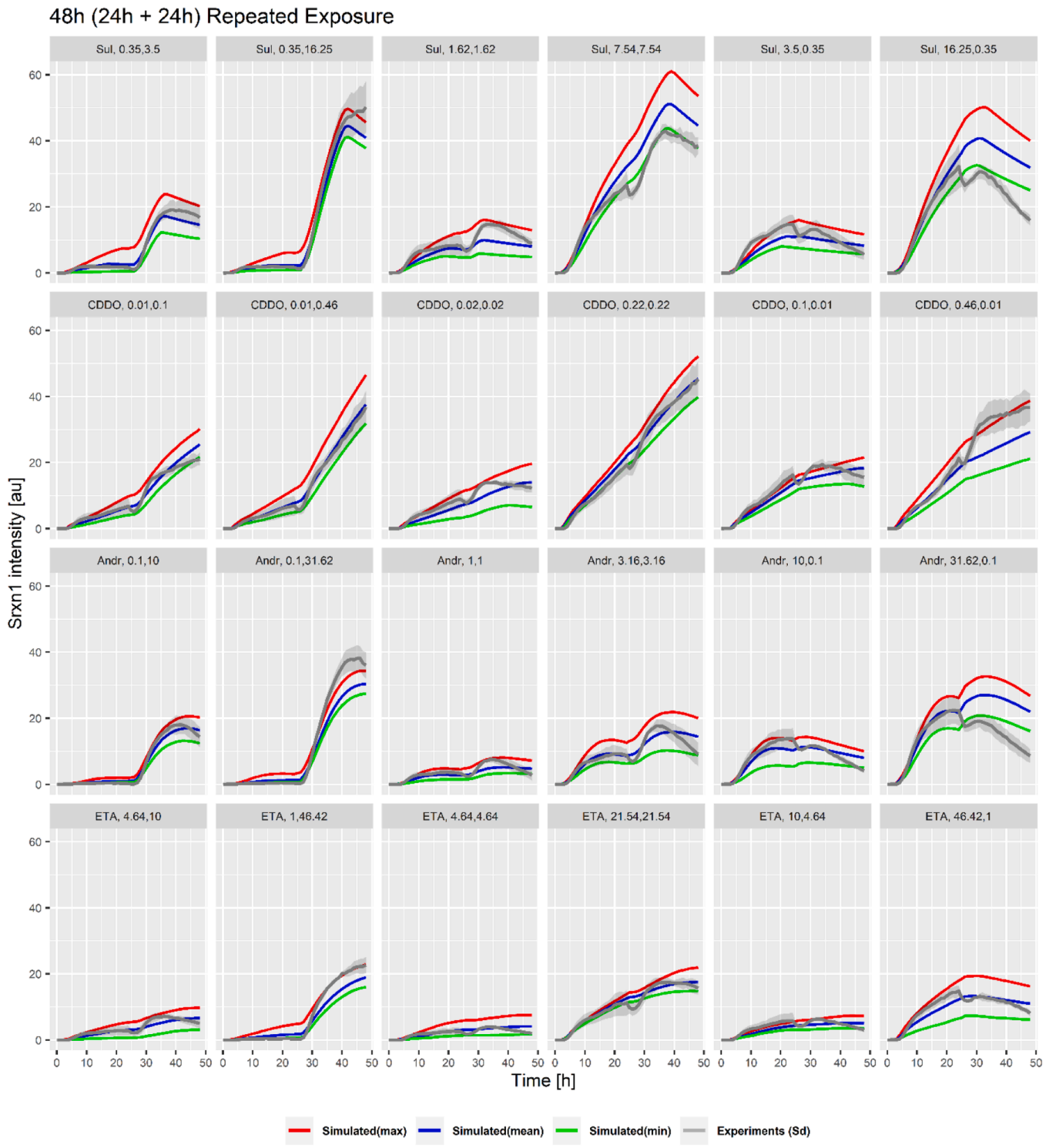

Fig. 6. Model with dynamic cofactor X describes SRXN1 dynamics following repeated exposure. Plots show simulated SRXN1 expression based on minimal (green), maximal (red) and mean (blue) NRF2 input per time point, and experimentally determined SRXN1 expression using HepG2 BAC-GFP reporter cells (shaded gray area: mean ± SD across three biological replicates) for 48 h (24 h + 24 h) repeated exposure scenarios. Each row corresponds to one chemical (Sul, Andr, ETA, and CDDO), with exposure levels during first and second exposure indicated above the panels, separated by a comma (in μM).

Besides the parameters determining the fraction of modified NRF2 over time, also the other parameters related to SRXN1 transcription and decay play an important role to determine NRF2-driven SRXN1 dynamics. We carried out a sensitivity analysis on the time-course simulations by varying the values of these parameters within a 0.5- and 2-fold range of the calibrated values to study how these parameters affect the temporal dynamics. To this purpose, we utilized the Sul-induced NRF2 inputs for the 48 h continuous exposure scenario. The parameters $V_{\max 1}$ (maximal transcription rate of SRXN1) and K_{m_u} (concentration of unmodified NRF2 at which the SRXN1 transcription rate is half-maximal) had qualitatively equal, yet opposite effects along the time course of the SRXN1 response (Fig. 7B-C). Interestingly, the parameter K_{m_m} (concentration of modified NRF2 at which the SRXN1 transcription rate is half-maximal) does not have any effect on the initial activation of

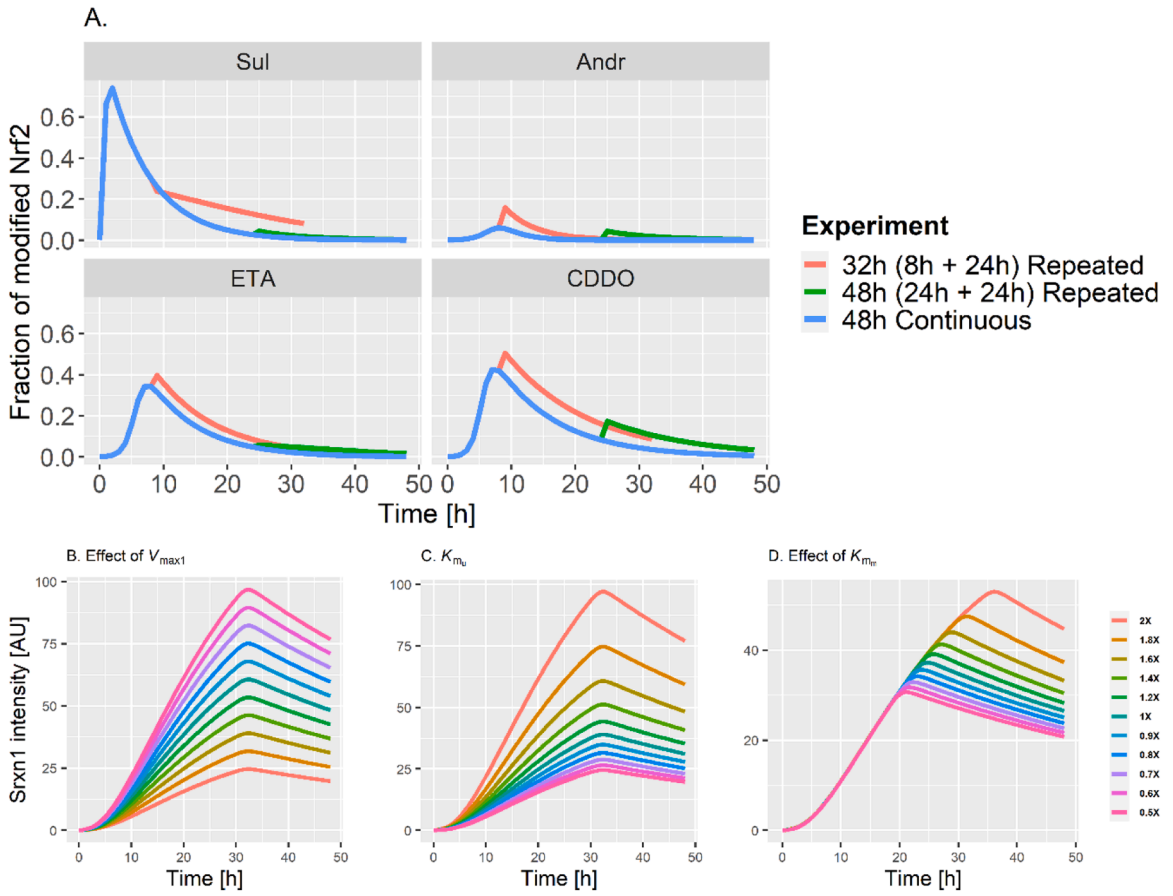

Fig. 7. The fraction of modified NRF2 (with high transcription factor activity) due to cofactor X varies over time, across chemicals and exposure scenario. A) The model-predicted fraction of modified NRF2 over time is plotted for 48 h continuous exposure (green), 32 h (8 h+24 h) repeated exposure (blue) and 48 h (24 h+24 h) repeated exposure (red). Chemicals are labeled at the top. B-D) Model-generated time profiles for the SRXN1 dynamics during the 48 h (24 h+24 h) Sul continuous exposure scenario by varying the parameter values within a 0.5- to 2-fold range from their optimal value in 10 steps: Each colored curve represents the predicted dynamics for one altered parameter, i.e., V_{max1} (B), K_{m_u} (C), and K_{m_m} (D). The effect of K_{m_m} modification is most pronounced at late time points, whereas K_{m_u} and V_{max1} have clear impact on the entire time course.

SRXN1 but only affects the late time point dynamics, with a higher K_{m_m} value leading to faster decay (Fig. 7D). This finding is likely caused by the strong initial increase in modified NRF2 predicted by the model fits, in combination with a K_{m_m} value that is estimated relatively low. In summary, the parameter K_{m_m} and the level of modified NRF2 over time jointly determine the SRXN1 response. Note that in a global sensitivity analysis we found all parameters to be sensitive (Fig. S19), with the magnitude of the total order sensitivity being slightly higher than the first order sensitivity, except for the Hill parameter n_u for SRXN1 transcription.

4. Discussion

In this study, we used live-cell imaging time course data for NRF2 and its downstream target SRXN1 in HepG2 BAC-GFP reporter cells exposed to various stressors and exposure conditions. By leveraging these quantitative data in a semi-mechanistic mathematical model, we investigated how the transcription factor activity of NRF2 is modulated by compound- and scenario-specific factors. This approach provided insight into the dynamic regulation of NRF2-mediated gene expression.

Our initial data analysis employing experimental NRF2-SRXN1 'hysteresis' plots already indicated a time-, chemical-, and exposure-dependent discrepancy between NRF2 and SRXN1 expression. The swift activation of NRF2 after compound exposure is in line with data suggesting that these compounds activate NRF2 at protein level by inhibiting its degradation through modification of Keap1 (Wakabayashi et al., 2004; Kobayashi et al., 2006). The observed delay in the onset of the SRXN1 response is likely due to the time it takes to transcribe and translate SRXN1 protein, and a similar delay in its return to baseline would be expected due to protein degradation dynamics. Interestingly, the maximal abundance of NRF2 achieved by Andr differed around 1-fold from that caused by Sul, yet the difference in maximal SRXN1 expression was almost 3-fold (at the highest concentration). However, CDDO exposure led to higher SRXN1 maximal expression compared to Sul (and other compounds) even though its NRF2 maximum was lower than for Sul. These experimental findings thus already hinted at factors in addition to the nuclear abundance of NRF2 playing a role in determining SRXN1 abundance.

In order to formally test whether the amount of NRF2 and its dynamics could be sufficient to explain SRXN1 abundance independent of treatment type, we developed a mathematical model with constant NRF2 transcription factor activity. Although this model could reasonably explain the Sul data for several concentrations, this approach was not successful for all concentrations and did not perform well when it was applied to the other three compounds. Thus, this finding clearly indicated that the NRF2-SRXN1 relationship obeyed a more complex mechanism than originally anticipated. This was confirmed by our final model incorporating dynamic, compound-dependent NRF2 modification (by cofactor X), which captured the observed SRXN1 dynamics across all scenarios well. This observation is in line with many reported studies suggesting that NRF2 activity depends on other factors or processes. Here, one important process is that NRF2 often forms

heterodimers with sMAF transcription factors (Rooney et al., 2020; Tonelli et al., 2018; Li et al., 2008). These heterodimers can also interact with other proteins that act as co-activators/co-suppressors to alter the transcription factor activity of NRF2-induced ARE gene expression. For instance, NRF2 is known to recruit p300 which modifies NRF2 by acetylation, resulting in an increase in NRF2's transcriptional abilities (Sun et al., 2009; Cai et al., 2015). On the other hand, methylation of NRF2 promoter residues, or microRNAs like miR153, miR27a, miR142–5p, and miR144 can result in inhibitory effects on NRF2-mediated transcription (Narasimhan et al., 2012; Su et al., 2013). It is thus likely that the disparity in SRXN1 expression among different treatments depends on factors that modulate NRF2 transcriptional regulation.

In our modeling framework, we used a Hill function to allow for a range of possible relationships between NRF2 and SRXN1, from linear to highly nonlinear, depending on the Hill coefficient (n) and the ratio of NRF2 to estimated K_m. In the simplest model version, the fitted Hill coefficient was close to 1 and the NRF2:K_m ratios remained much smaller than 1, corresponding to a nearly linear regime. This indicates that for these conditions, SRXN1 expression responds in a graded, proportional manner to NRF2, without strong ultrasensitivity or threshold effects. However, in our most complex where the fraction of modified NRF2 changes dynamically over time, we observed a marked difference: the Hill coefficient for the modified NRF2 form was close to 10 (highly nonlinear/ultrasensitive), while for the unmodified form it remained near 1. This supports the idea that cofactor-mediated modification of NRF2 can drive strong nonlinearities in downstream gene regulation, even when the unmodified form acts linearly.

Consistent with the improved model fit for the model with a dynamic cofactor X compared to the model with constant NRF2 transcription factor activity, the fraction of modified NRF2 was indeed predicted to exhibit large variation in the rate and extent of modified NRF2 across treatment type and exposure scenario. This suggests that in response to Andr, only a low fraction of NRF2 becomes modified. This would explain why Andr- and Sul-induced NRF2 induction is similar whereas the SRXN1 expression in response to these two compounds is very different. Further analysis of the developed model revealed that the parameter K_a controls the SRXN1 dynamics only at late time points. This coincides with the dynamics of the fraction of modified NRF2 that is predicted to quickly decrease during the late response. Differences in the fractions of modified NRF2 over time across compounds could be due to differences in the in-vitro half-lives of the compounds, which may directly affect other pathways or cofactors that mediate the NRF2 transcription factor activity. Indeed, in our related paper we show that NRF2 response activation is very much dependent on compound kinetics (Hiemstra et al., 2022).

Beyond compound kinetics, additional mechanisms may contribute to the observed compound-dependent effects on SRXN1 regulation. For example, certain compounds may differentially activate specific xenobiotic nuclear receptors such as AhR, CAR, or PXR, leading to receptor crosstalk and modulation of NRF2 signaling (Vorrink and Domann, 2014). Differences in metabolic processing, resulting in the formation of distinct reactive metabolites, may also influence the magnitude or duration of NRF2 activation and downstream gene induction (Hayes and Dinkova-Kostova, 2014). Furthermore, some compounds may selectively induce either oxidative or electrophilic stress, each of which can recruit different upstream signaling pathways or cofactor proteins. Variability in cellular uptake, efflux, or subcellular localization could further contribute to the distinct transcriptional responses observed (Klaassen and Aleksunes, 2010). Elucidating the precise mechanisms underlying compound dependency will require future studies integrating metabolic profiling, receptor activation assays, and targeted perturbations of relevant signaling pathways.

Although this has not been experimentally shown in great detail, it is known that NRF2 can sense stress differentially depending on contextualized regulatory mechanisms following ligand and treatment type. For instance, Rong et al. reported that tert- butylhydroquinone (tBHQ) and Sul induce changes in NRF2 transcription factor activity related to Raf-1 kinase activity (Yu et al., 1999). In another study in rats, copper induced SRXN1 expression via NF-kB signaling, hinting at the potential importance of crosstalk (Jeong et al., 2012). As a third example, a heterodimer formed by ligand-bound PPARγ and RXR enhances the strength of glutathione *S*-transferase expression by facilitating transactivation complexes comprising NRF2 and C/EBPβ (Park et al., 2004). Finally, Sul-induced NQO1 expression is not linked to altered cellular levels of NRF2, yet is associated with oscillatory changes in cytoplasmic/nuclear translocation of NRF2, which is also linked to ongoing phosphorylation and dephosphorylation of NRF2 via a non-canonical pathway (Xue et al., 2015). Future studies are required that aim to determine the contribution of specific cofactors recruited by NRF2, of non-canonical pathways influencing NRF2, and how these contributions vary over time and with type of exposure. While our current model captures compound- and time-dependent modulation of NRF2 activity through an empirical dynamic cofactor term, other mechanistic model structures—such as explicit feedback loops or dose-dependent feedback mechanisms—could also be considered. Future model extensions may incorporate these forms when quantitative time-course data for relevant cofactors or signaling intermediates become available. We chose our stepwise, data-driven approach to balance model complexity and interpretability in light of the current data. In order to confirm our hypothesis that such cofactors and pathways jointly affect NRF2 modification, the influence of silencing of the identified factors on NRF2 and SRXN1 dynamics need to be evaluated. Although our final model can explain SRXN1 dynamics driven by NRF2 for four different compounds, the current model is limited because it requires NRF2 measurements to translate these into downstream SRXN1 dynamics. This limitation might be overcome in the future by extending the model to include in vitro compound kinetics, and predicting NRF2 based on those kinetics. Such modeling will likely reveal additional mechanistic information about NRF2 pathway signaling dynamics beyond the link between NRF2 and SRXN1 that we focused on with our current models.

In summary, in our work we aimed to explain SRXN1 differential expression dynamics given a particular input of NRF2 dynamics. To this purpose, we developed a nonlinear mixed effect semi-mechanistic modeling approach, and applied this to HepG2 BAC-GFP experimental data on NRF2 and SRXN1 that were acquired under multiple compound exposure scenarios (Niemeijer et al., 2025). Our proposed hierarchical model for a subset of parameters quantified factors that change NRF2 transcription factor activity inducing SRXN1 expression. Likely these underlying mechanisms are highly important to tightly regulate the NRF2 transcriptional machinery and thereby the downstream targets that are required to maintain the balance in the cellular environment. We focused on SRXN1 only in our model analysis, yet we expect that the general concept extrapolates to other downstream NRF2 targets, which would require measurements on those targets as well as model extensions. For example, through application of mathematical models to experimental data we recently showed that also the relation between nuclear NRF2 presence and glutathione abundance, an important antioxidant, is compound-dependent (Perkins et al., 2019). Although glutathione is not a direct NRF2 target, its formation is affected by glutamate cysteine ligase (GCL), whose catalytic (GCLC) and modifier (GCLM) subunits are both transcriptional targets of NRF2 (Spinu et al., 2020). A recent human transcriptome study showed that SRXN1 is an excellent downstream biomarker of NRF2 activation to study chemical toxicity (Rooney et al., 2020). Therefore, quantitative knowledge on the link between NRF2 and SRXN1 could be very useful for predicting the threshold between cellular adaptivity and adversity. Especially the detailed dynamics of NRF2 and SRXN1, and cofactors determining NRF2 transcription factor activity, are likely important drivers of cell fate. One way to achieve such predictions on adversity includes the application of quantitative adverse outcome pathways (qAOPs) for chemical risk assessment. In such qAOPs, the relationship between Molecular

initiating events (MIEs; for the compounds investigated here this could be described by e.g. 'chemical-induced electrophilic attack on KEAP1 cysteine residues') and key events (KEs; for the investigated compounds this could be described as e.g. NRF2 activation and SRXN1 induction, or more crudely as oxidative stress) is generally considered to be very direct (Perkins et al., 2019; Spinu et al., 2020). We show that such relationships, even of close-by events, may be more complicated than originally anticipated, which implies that detailed experimental studies on NRF2 binding partners and cofactors are required to fully take advantage of qAOPs for risk assessment purposes in the future. Nevertheless, in the absence of full mechanistic understanding of the NRF2-SRXN1 relation, our current models can already be incorporated within such qAOPs.

CRediT authorship contribution statement

Joost B Beltman: Writing – review & editing, Supervision, Project administration, Funding acquisition, Conceptualization. **Bob van de Water:** Writing – review & editing, Supervision, Funding acquisition, Conceptualization. **Alistair M Middleton:** Writing – review & editing, Supervision, Conceptualization. **Marije Niemeijer:** Writing – review & editing, Methodology, Investigation. **Andrew White:** Writing – review & editing, Supervision, Conceptualization. **Liesanne Loonstra-Wolters:** Writing – review & editing, Methodology, Investigation. **Bas ter Braak:** Writing – review & editing, Methodology, Investigation. **Raju Prasad Sharma:** Writing – original draft, Visualization, Software, Methodology, Investigation, Formal analysis, Data curation, Conceptualization.

Declaration of Competing Interest

The authors declare the following financial interests/personal relationships which may be considered as potential competing interests: Bob van de Water reports financial support was provided by Unilever SERS. Joost Beltman reports financial support was provided by Unilever SERS. Andrew White reports a relationship with Unilever SERS that includes: employment. Alistair Middleton reports a relationship with Unilever SERS that includes: employment. The HepG2 BAC GFP reporters are currently licensed to Toxys. BtB is currently employed at this company. If there are other authors, they declare that they have no known competing financial interests or personal relationships that could have appeared to influence the work reported in this paper.

Acknowledgements

This work was supported by a Unilever SERS research grant.

Appendix A. Supporting information

Supplementary data associated with this article can be found in the online version at doi:10.1016/j.tox.2025.154284.

Data availability

The code to run the presented mathematical models is available at https://doi.org/10.5281/zenodo.17181465 (released on 23 September 2025).

References

Abbas, K., Riquier, S., Drapier, J.C., 2013. Peroxiredoxins and Sulfiredoxin at the Crossroads of the NO and H 2O2 Signaling Pathways, 1st ed., 527. Elsevier Inc. https://doi.org/10.1016/B978-0-12-405882-8.00006-4.

Bischoff, L.J.M., Kuijper, I.A., Schimming, J.P., et al., 2019. A systematic analysis of Nrf2 pathway activation dynamics during repeated xenobiotic exposure. Arch. Toxicol. 93 (2), 435–451. https://doi.org/10.1007/s00204-018-2353-2.

Bloom, D.A., Jaiswal, A.K., 2003. Phosphorylation of Nrf2 at Ser40 by protein kinase c in response to antioxidants leads to the release of Nrf2 from INrf2, but is not required for Nrf2 stabilization/accumulation in the nucleus and transcriptional activation of antioxidant response element. J. Biol. Chem. 278 (45), 44675–44682. https://doi.org/10.1074/jbc.M307633200.

Bois, F.Y., Maszle, D.R., 1997. MCSim: a Monte Carlo simulation program. J. Stat. Softw. 2 (9). https://doi.org/10.18637/jss.v002.i09.

ter Braak, B., Klip, J.E., Wink, S., et al., 2022. Mapping the dynamics of Nrf2 antioxidant and NFκB inflammatory responses by soft electrophilic chemicals in human liver cells defines the transition from adaptive to adverse responses. Toxicol. Vitr. 84 (January), 105419. https://doi.org/10.1016/j.tiv.2022.105419.

Cai, D., Yin, S., Yang, J., Jiang, Q., Cao, W., 2015. Histone deacetylase inhibition activates Nrf2 and protects against osteoarthritis. Arthritis Res. Ther. 17 (1), 269. https://doi.org/10.1186/s13075-015-0774-3.

Centers, C., States, U., Ostapowicz, G., et al., 2002. Article results of a prospective study of acute liver failure at 17 tertiary. Ann. Intern. Med. 15, 947–955.

Eggler, A.L., Liu, G., Pezzuto, J.M., van Breemen, R.B., Mesecar, A.D., 2005. Modifying specific cysteines of the electrophile-sensing human Keap1 protein is insufficient to disrupt binding to the Nrf2 domain Neh2. Proc. Natl. Acad. Sci. 102 (29), 10070–10075. https://doi.org/10.1073/pnas.0502402102.

Ghanim, B., Ahmad, M., Abdallah, Q., Qatouseh, L., Qinna, N., 2021. Modulation of NRF2/ARE pathway- and cell death-related genes during drug-induced liver injury. Hum. Exp. Toxicol. 40 (12), 2223–2236. https://doi.org/10.1177/09603271211027947.

Hayes, J.D., Dinkova-Kostova, A.T., 2014. The Nrf2 regulatory network provides an interface between redox and intermediary metabolism. Trends Biochem. Sci. 39 (4), 199–218. https://doi.org/10.1016/j.tibs.2014.02.002.

Hiemstra, S., Fehling-Kaschek, M., Kuijper, I.A., et al., 2022. Dynamic modeling of Nrf2 pathway activation in liver cells after toxicant exposure. Sci. Rep. 12 (1), 7336. https://doi.org/10.1038/s41598-022-10857-x.

Hsieh, N.H., Reisfeld, B., Chiu, W.A., 2020. Pksensi: an R package to apply global sensitivity analysis in physiologically based kinetic modeling. SoftwareX 12, 100609. https://doi.org/10.1016/j.softx.2020.100609.

Huang, H.C., Nguyen, T., Pickett, C.B., 2000. Regulation of the antioxidant response element by protein kinase C-mediated phosphorylation of NF-E2-related factor 2. Proc. Natl. Acad. Sci. USA 97 (23), 12475–12480. https://doi.org/10.1073/pnas.220418997.

Huang, H.C., Nguyen, T., Pickett, C.B., 2002. Phosphorylation of Nrf2 at Ser-40 by protein kinase c regulates antioxidant response element-mediated transcription. J. Biol. Chem. 277 (45), 42769–42774. https://doi.org/10.1074/jbc.M206911200.

Itoh K., Chiba T., Takahashi S., et al. An Nrf2 / Small Maf Heterodimer Mediates the Induction of Phase II Detoxifying Enzyme Genes through Antioxidant Response Elements. 1997;322(236):313-322.

Jeong, W., Bae, S.H., Toledano, M.B., Rhee, S.G., 2012. Role of sulfiredoxin as a regulator of peroxiredoxin function and regulation of its expression. Free Radic. Biol. Med. 53 (3), 447–456. https://doi.org/10.1016/j.freeradbiomed.2012.05.020.

Jose, E., March-Steinman, W., Wilson, B.A., et al., 2024. Temporal coordination of the transcription factor response to H2O2 stress. Nat. Commun. 15 (1), 3440. https://doi.org/10.1038/s41467-024-47837-w.

Kaplowitz, N., 2001. Drug-induced liver disorders: implications for drug development and regulation. Drug Saf. 24 (7), 483–490. https://doi.org/10.2165/00002018-200124070-00001.

Kataoka, K., Igarashi, K., Itoh, K.E.N., et al., 1995. Small maf proteins heterodimerize with fos and may act as competitive repressors of the NF-E2 transcription factor. Mol. Cell Biol. 15 (4), 2180–2190.

Katsuoka, F., Motohashi, H., Engel, J.D., Yamamoto, M., 2005. Nrf2 transcriptionally activates the mafg gene through an antioxidant response element. J. Biol. Chem. 280 (6), 4483–4490. https://doi.org/10.1074/jbc.M411451200.

Katsuoka, F., Yamamoto, M., 2016. Small maf proteins (MafF, MafG, MafK): history, structure and function. Gene 586 (2), 197–205. https://doi.org/10.1016/j.gene.2016.03.058.

Ke, Q., Yang, J., Liu, H., et al., 2021. Dose- and time-effects responses of nonylphenol on oxidative stress in rat through the Keap1-Nrf2 signaling pathway. Ecotoxicol. Environ. Saf. 216, 112185. https://doi.org/10.1016/j.ecoenv.2021.112185.

Khalil, H.S., Goltsov, A., Langdon, S.P., Harrison, D.J., Bown, J., Deeni, Y., 2015. Quantitative analysis of NRF2 pathway reveals key elements of the regulatory circuits underlying antioxidant response and proliferation of ovarian cancer cells. J. Biotechnol. 202, 12–30. https://doi.org/10.1016/j.jbiotec.2014.09.027.

Klaassen, C.D., Aleksunes, L.M., 2010. Xenobiotic, bile acid, and cholesterol transporters: function and regulation. Pharm. Rev. 62 (1), 1–96. https://doi.org/10.1124/pr.109.002014.

Kobayashi, A., Kang, M.-I., Watai, Y., et al., 2006. Oxidative and electrophilic stresses activate Nrf2 through inhibition of ubiquitination activity of Keap1. Mol. Cell Biol. 26 (1), 221–229. https://doi.org/10.1128/MCB.26.1.221-229.2006.

Leclerc, E., Hamon, J., Claude, I., Jellali, R., Naudot, M., Bois, F., 2015. Investigation of acetaminophen toxicity in HepG2/C3a microscale cultures using a system biology model of glutathione depletion. Cell Biol. Toxicol. 31 (3), 173–185. https://doi.org/10.1007/s10565-015-9302-0.

Li, W., Yu, S., Liu, T., et al., 2008. Heterodimerization with small maf proteins enhances nuclear retention of Nrf2 via masking the NESzip motif. Biochim. Biophys. Acta Mol. Cell Res. 1783 (10), 1847–1856. https://doi.org/10.1016/j.bbamcr.2008.05.024.

Louizos, C., Yáñez, J.A., Forrest, M.L., Davies, N.M., 2014. Understanding the hysteresis loop conundrum in pharmacokinetic/pharmacodynamic relationships. J. Pharm. Pharm. Sci. 17 (1), 34–91. ⟨https://pubmed.ncbi.nlm.nih.gov/24735761⟩.

Ma, Q., 2013. Role of Nrf2 in oxidative stress and toxicity. Annu Rev. Pharm. Toxicol. 53 (1), 401–426. https://doi.org/10.1146/annurev-pharmtox-011112-140320.

Kolodkin, A.N., Sharma, R.P., Colangelo, A.M., et al., 2020. ROS networks: designs, aging, Parkinson's disease and precision therapies. npj Syst. Biol. Appl. 6 (1). https://doi.org/10.1038/s41540-020-00150-w.

Narasimhan, M., Patel, D., Vedpathak, D., Rathinam, M., Henderson, G., Mahimainathan, L., 2012. Identification of novel microRNAs in post-transcriptional control of Nrf2 expression and redox homeostasis in neuronal, SH-SY5Y cells. PLoS One 7 (12). https://doi.org/10.1371/journal.pone.0051111.

Niemeijer, M., Wolters, L., ter Braak, B., et al., 2025. Imaging-based temporal dynamics of electrophile-induced NRF2 signaling in liver cells identifies adaptive versus adverse repeated exposure conditions. bioRxiv. https://doi.org/10.1101/2025.08.22.671761.

Park, E.Y., Cho, I.J., Kim, S.G., 2004. Transactivation of the PPAR-responsive enhancer module in chemopreventive glutathione S-transferase gene by the peroxisome proliferator-activated receptor-γ and retinoid x receptor heterodimer. Cancer Res. 64 (10), 3701–3713. https://doi.org/10.1158/0008-5472.CAN-03-3924.

Perkins, E.J., Ashauer, R., Burgoon, L., et al., 2019. Building and applying quantitative adverse outcome pathway models for chemical hazard and risk assessment. Environ. Toxicol. Chem. 38 (9), 1850–1865. https://doi.org/10.1002/etc.4505.

Pickering, A.M., Vojtovich, L., Tower, J., A Davies, K.J., 2013. Oxidative stress adaptation with acute, chronic, and repeated stress. Free Radic. Biol. Med. 55, 109–118. https://doi.org/10.1016/j.freeradbiomed.2012.11.001.

Qian, Z., Zhou, T., Gurguis, C.I., et al., 2015. Nuclear factor, erythroid 2-like 2-associated molecular signature predicts lung cancer survival. Sci. Rep. 5. https://doi.org/10.1038/srep16889.

Reichard, J.F., Motz, G.T., Puga, A., 2007. Heme oxygenase-1 induction by NRF2 requires inactivation of the transcriptional repressor BACH1. Nucleic Acids Res. 35 (21), 7074–7086. https://doi.org/10.1093/nar/gkm638.

Rooney, J.P., Chorley, B., Hiemstra, S., et al., 2020. Mining a human transcriptome database for chemical modulators of NRF2. PLoS One 15 (9 September), 1–26. https://doi.org/10.1371/journal.pone.0239367.

Spinu, N., Cronin, M.T.D., Enoch, S.J., Madden, J.C., Worth, A.P., 2020. Quantitative adverse outcome pathway (qAOP) models for toxicity prediction. Arch. Toxicol. 94 (5), 1497–1510. https://doi.org/10.1007/s00204-020-02774-7.

Sun, Z., Chin, Y.E., Zhang, D.D., 2009. Acetylation of Nrf2 by p300/CBP augments promoter-specific DNA binding of Nrf2 during the antioxidant response. Mol. Cell Biol. 29 (10), 2658–2672. https://doi.org/10.1128/mcb.01639-08.

Suzuki, T., Yamamoto, M., 2015. Molecular basis of the Keap1-Nrf2 system. Free Radic. Biol. Med. 88 (Pt B), 93–100. https://doi.org/10.1016/j.freeradbiomed.2015.06.006.

Su, Z.Y., Khor, T.O., Shu, L., et al., 2013. Epigenetic reactivation of Nrf2 in murine prostate cancer TRAMP C1 cells by natural phytochemicals Z-ligustilide and radix angelica sinensis via promoter CpG demethylation. Chem. Res. Toxicol. 26 (3), 477–485. https://doi.org/10.1021/tx300524p.

Tonelli, C., Chio, I.I.C., Tuveson, D.A., 2018. Transcriptional regulation by Nrf2. Antioxid. Redox Signal 29 (17), 1727–1745. https://doi.org/10.1089/ars.2017.7342.

Vehtarh, A., Gelman, A., Simpson, D., Carpenter, B., Burkner, P.C., 2021. Rank-Normalization, folding, and localization: an improved (Formula presented) for assessing convergence of MCMC (with Discussion)*†. Bayesian Anal. 16 (2), 667–718. https://doi.org/10.1214/20-BA1221.

Vorrink, S.U., Domann, F.E., 2014. Regulatory crosstalk and interference between the xenobiotic and hypoxia sensing pathways at the AhR-ARNT-HIF1α signaling node. Chem. Biol. Interact. 218, 82–88. https://doi.org/10.1016/j.cbi.2014.05.001.

Wakabayashi, N., Dinkova-Kostova, A.T., Holtzclaw, W.D., et al., 2004. Protection against electrophile and oxidant stress by induction of the phase 2 response: fate of cysteines of the Keap1 sensor modified by inducers. Proc. Natl. Acad. Sci. 101 (7), 2040–2045. https://doi.org/10.1073/pnas.0307301101.

Wijaya, L.S., Rau, C., Braun, T.S., et al., 2022. Stimulation of de novo glutathione synthesis by nitrofurantoin for enhanced resilience of hepatocytes. Cell Biol. Toxicol. 38 (5), 847–864. https://doi.org/10.1007/s10565-021-09610-3.

Wink, S., Hiemstra, S., Herpers, B., van de Water, B., 2017. High-content imaging-based BAC-GFP toxicity pathway reporters to assess chemical adversity liabilities. Arch. Toxicol. 91 (3), 1367–1383. https://doi.org/10.1007/s00204-016-1781-0.

Wink, S., Hiemstra, S.W., Huppelschoten, S., Klip, J.E., Water, B., Van De, 2018. Dynamic imaging of adaptive stress response pathway activation for prediction of drug induced liver injury. Arch. Toxicol. 92 (5), 1797–1814. https://doi.org/10.1007/s00204-018-2178-z.

Xue, M., Momiji, H., Rabbani, N., et al., 2015. Frequency modulated translocational oscillations of Nrf2 mediate the antioxidant response element cytoprotective transcriptional response. Antioxid. Redox Signal 23 (7), 613–629. https://doi.org/10.1089/ars.2014.5962.

Yamamoto, M., Kensler, T.W., Motohashi, H., 2018. The KEAP1-NRF2 system: a thiol-based sensor-effector apparatus for maintaining redox homeostasis. Physiol. Rev. 98 (3), 1169–1203. https://doi.org/10.1152/physrev.00023.2017.

Yu, R., Lei, W., Mandlekar, S., et al., 1999. Role of a mitogen-activated protein kinase pathway in the induction of phase II detoxifying enzymes by chemicals. J. Biol. Chem. 274 (39), 27545–27552. https://doi.org/10.1074/jbc.274.39.27545.

Zhang, Q., Andersen, M.E., 2007. Dose response relationship in anti-stress gene regulatory networks. PLoS Comput. Biol. 3 (3), 0345–0363. https://doi.org/10.1371/journal.pcbi.0030024.

Zipper, L.M., Mulcahy, R.T., 2000. Inhibition of ERK and p38 MAP kinases inhibits binding of Nrf2 and induction of GCS genes. Biochem. Biophys. Res. Commun. 278 (2), 484–492. https://doi.org/10.1006/bbrc.2000.3830.